ADVANCES IN ATMOSPHERIC SCIENCES, VOL. 30, NO. 5, 2013, 1331–1342

Performances of Seven Datasets in Presenting the Upper Ocean Heat Content in the South China Sea

CHEN Xiao[1,2] (陈 晓), YAN Youfang[1] (严幼芳), CHENG Xuhua[1] (程旭华), and QI Yiquan*[1] (齐义泉)

[1] *State Key Laboratory of Tropical Oceanography, South China Sea Institute of Oceanology, Chinese Academy of Sciences, Guangzhou* 510301

[2] *University of Chinese Academy of Sciences, Beijing* 100049

(Received 28 June 2012; revised 23 November 2012; accepted 18 January 2013)

ABSTRACT

In this study, the upper ocean heat content (OHC) variations in the South China Sea (SCS) during 1993–2006 were investigated by examining ocean temperatures in seven datasets, including World Ocean Atlas 2009 (WOA09) (climatology), Ishii datasets, Ocean General Circulation Model for the Earth Simulator (OFES), Simple Ocean Data Assimilation system (SODA), Global Ocean Data Assimilation System (GODAS), China Oceanic ReAnalysis system （CORA）, and an ocean reanalysis dataset for the joining area of Asia and Indian–Pacific Ocean (AIPO1.0). Among these datasets, two were independent of any numerical model, four relied on data assimilation, and one was generated without any data assimilation. The annual cycles revealed by the seven datasets were similar, but the interannual variations were different. Vertical structures of temperatures along the 18°N, 12.75°N, and 120°E sections were compared with data collected during open cruises in 1998 and 2005–08. The results indicated that Ishii, OFES, CORA, and AIPO1.0 were more consistent with the observations. Through systematic comparisons, we found that each dataset had its own shortcomings and advantages in presenting the upper OHC in the SCS.

Key words: South China Sea, ocean heat content, multiple datasets, interannual variability

Citation: Chen, X., Y. F. Yan, X. H. Cheng, and Y. Q. Qi, 2013: Performances of seven datasets in presenting the upper ocean heat content in the South China Sea. *Adv. Atmos. Sci.*, **30**(5), 1331–1342, doi: 10.1007/s00376-013-2132-1.

1. Introduction

Late in the 20th century, the changes in Earth's heat balance were influenced significantly by the changes in ocean heat content (OHC) (Levitus et al., 2001). In recent decades, extensive efforts have been devoted to understand the role of the global OHC variability, particularly the upper OHC, in the changes of the climate system (Domingues et al., 2008; Douglass and Knox, 2009; Levitus et al., 2009). However, the global OHC variability is not the only factor to be considered; the marginal seas also have their own characteristic influences (Yan et al., 2010b; Na et al., 2012).

The South China Sea (SCS) is the largest marginal sea located in the northwest Pacific Ocean, with an average depth of 1800 m and a maximum depth of over 5400 m. It connects with the Java Sea and the Sulu Sea through shallow passages in the south, and with the Pacific Ocean through the Luzon Strait in the north (Fig. 1). Because of its special location, the SCS is affected by three major summer monsoons: the western North Pacific summer monsoon, the East Asian subtropical monsoon, and the Indian summer monsoon (Wang and Wu, 1997). Such a complicated geographical background makes the upper OHC variations in the SCS relatively complex (Qu et al., 2004; Yan et al., 2010b). Moreover, these variations exert influence on local atmospheric circulations, formation of tropical cyclones (Wang et al., 2007), burst of monsoon (Lai et al., 2011), and sea level variations (Cheng and Qi, 2007; Rong et al., 2007). Thus, it is particularly

*Corresponding author: QI Yiquan, qiyiquan@scsio.ac.cn

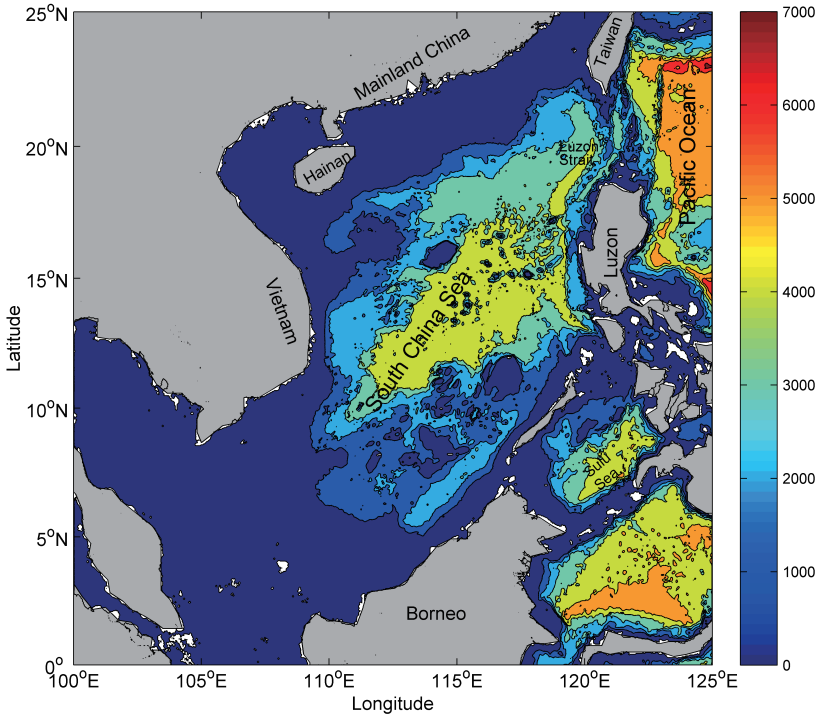

Fig. 1. Bottom topography of the SCS (data from http://www.ngdc.noaa.gov/mgg/global/relief/ETOPO2/ETOPO2v2-2006/) (units: m).

important to study the upper OHC variations in the SCS.

Tentative explorations have been made to understand the upper OHC variations in the SCS using different datasets. Employing temperature profiles that were generated from more than 62 000 stations during 1959–88, He and Guan (1997) studied the interannual and decadal modifications of the upper OHC (vertically averaged temperature of upper 100 m) in the SCS. Tong et al. (2006) calculated the upper OHC in the SCS using the merged altimetric data, based on the linear relationship between the sea level anomaly (SLA) and OHC variations. Using the Ishii datasets (Ishii et al., 2006), the interannual variations of the upper OHC in the SCS and its response to ENSO have been investigated (Cheng and Qi, 2007; Rong et al., 2007; Yan et al., 2010b). Overall, owing to the distinctive characteristics of each dataset, findings of the previous studies about the upper OHC variations in the SCS, especially the interannual variations, were somehow different. Therefore, the sources of uncertainties in these datasets need to be explored systematically.

As we know, oceanographers rely much on ocean datasets, including ocean reanalysis datasets, model products, and those compiled from realistic observations. However, these datasets contain considerable uncertainties, especially in estimating the subsurface oceanic state (Zhu et al., 2011). Efforts have been made to validate and verify the performances of different global ocean model products in presenting the global OHC variations (Carton and Santorelli, 2008; Lyman et al., 2010; Zhu et al., 2011). While the processes in the global oceans attract more attention, the marginal seas are less considered. It is worthy to select suitable datasets that can reveal the upper OHC variations in the SCS more accurately. So far, few studies have been conducted to estimate the performances of different datasets in presenting the upper OHC in the SCS. In this study, seven datasets were validated by examining their performances in presenting the upper OHC in the SCS, including climatology and interannual variations. A Taylor diagram was adopted to compare the performances of these datasets; comparisons with *in situ* hydrologic data along selected sections were also performed.

The rest of the paper is arranged as follows. Section 2 describes the data and data processing. Section 3 presents a series of comparisons of the upper OHC variations in the SCS using the seven datasets. Summary is given in section 4.

2. Datasets and methodology

In the present study, the performances of seven datasets of subsurface ocean temperature in presenting the upper OHC in the SCS were verified. These

Table 1. Datasets considered in this study

Analysis name	Time span (year)	Model	Resolution (lon×lat)	Maximum depth (m)	Assimilation method	Country
WOA09	Climatology	None	1°×1° 24 levels	1500	Objective analysis	USA
ISHII	1945–2010	None	1°×1° 24 levels	1500	Objective analysis	Japan
OFES	1950–2006	MOM3	0.5°×0.5° 54 levels	6065	None	Japan
SODA	1958–2008	MOM2	0.5°×0.5° 40 levels	5374	OI	USA
GODAS	1980–2010	MOM3	1°×1/3° 40 levels	4478	3DVAR	USA
CORA	1986–2008	POMgcs	0.5°×0.5° 24 levels	5000	3DVAR	China
AIPO1.0	1993–2006	HYCOM	1/4°×1/4° 33 levels	5500	EnOI	China

seven datasets are as follows: Ishii, World Ocean Atlas 2009 (WOA09), Ocean General Circulation Model for the Earth Simulator (OFES), Simple Ocean Data Assimilation system (SODA), Global Ocean Data Assimilation System (GODAS), China Oceanic ReAnalysis system (CORA), and an ocean reanalysis dataset for the joining area of Asia and Indian–Pacific Ocean (AIPO1.0). Basic information of these datasets is given in Table 1 and Table 2.

The WOA09 dataset used in this study is a climatology dataset of the National Oceanographic Data Center of the National Ocean and Atmosphere Administrations (NODC/NOAA). The ocean temperature–salinity dataset produced by Ishii et al. (2006) (hereafter Ishii; http://dss.ucar.edu/datasets/ds285.3/) was created by objective analysis. The source data of

Table 2. Vertical levels of upper 300 m of these datasets (units: m)

WOA09	Ishii	OFES	SODA	GODAS	CORA	AIPO1.0
0	0	2.5	5.01	5	2.5	5
10	10	7.6	15.07	15	10	10
20	20	12.8	25.28	25	30	20
30	30	18.4	35.76	35	50	30
50	50	24.3	46.61	45	100	50
75	75	30.8	51.98	55	150	75
100	100	37.8	70.02	65	200	100
125	125	45.6	82.92	75	250	125
150	150	54.0	96.92	85	300	150
200	200	63.2	112.32	95		200
250	250	73.2	129.49	105		250
300	300	84.0	148.96	115		300
		95.6	171.4	125		
		107.8	197.79	135		
		120.8	229.48	145		
		134.3	268.46	155		
		148.4		165		
		162.8		175		
		177.6		185		
		192.5		195		
		207.5		205		
		223.2		215		
		240.9		225		
		261.9		238		
		287.5		262		
				303		

Ishii consisted of the global temperature–salinity in the tropical Pacific from IRD (L'institut de recherché pour le development, France), World Ocean Database/Atlas 2005 (WOD05/WOA05) and the Centennial *in situ* Observation-Based Estimates (COBE) SST, Array for Real-time Geostrophic Oceanography (Argo) profiles, and the latest Global Temperature–Salinity Profile Program (GTSPP) datasets. The analysis scheme that Ishii adopted was based on a variational minimization with spatiotemporal covariance of background error (Ishii et al., 2006).

OFES products were based on the Modular Ocean Model version 3 (MOM3). The quasiglobal, eddy-resolving model products had various versions with different time and space resolutions (Sasaki et al., 2004; Yoshikazu Sasai et al., 2004; Masumoto et al., 2004; Sasaki et al., 2006). The surface momentum fluxes that OFES utilized were reanalysis products from the National Center for Enviornmental Prediction and the National Center for Atmospheric Research (NCEP/NCAR) (Kalnay et al., 1996) or products from Quik Scatterometer (QuikSCAT) (Kubotam et al., 2002). OFES adopted the bulk formula of Rosati and Miyakoda (1988) for calculating the surface heat flux calculation. Considering the actual need of application, we chose the monthly version with a horizontal resolution of $0.5^\circ \times 0.5^\circ$, whose surface momentum fluxes were obtained from the NCEP/NCAR reanalysis dataset.

SODA reanalysis (Carton and Giese, 2008) is a monthly reanalysis product covering nearly the global oceans. The source data used in SODA included WOA05, GTSPP, and in situ and Advanced Very High Resolution Radiometer (AVHRR) SST. Its surface fluxes included ERA-40 and QuikSCAT winds, Global Precipitation Climatology Project rain, and bulk heat flux. SODA adopted MOM2 and optimal interpolation (OI) as its ocean model and assimilation scheme, respectively.

The ocean model and assimilation method adopted by GODAS were MOM3 and three-dimensional variational data assimilation (3DVAR), respectively (Behringer, 2005). The standard assimilation datasets used in GODAS included WOD98, GTSPP, moored temperature, Argo profiles, and altimeter sea level datasets. Its surface fluxes included the wind fields and fluxes from the NCEP and NCEP-2 datasets.

CORA, produced by National Marine Data and Information Service (NMDIS), focuses on the China coastal water and adjacent regions. This reanalysis system was based on the Princeton Ocean Model with a generalized coordinate system (POMgcs) that used the multigrid 3DVAR scheme for data assimilation (http://www.cora.net.cn). In this study, we choose its monthly version with a horizontal resolution of $0.5^\circ \times 0.5^\circ$. The temperature–salinity profiles used in CORA contained not only WOD05, GTSPP, and Argo profiles, but also Nansen bottles, conductivity–temperature–depth (CTD) recorder, and bathythermograph (BT) data, which were collected from NMDIS. The SLA data used in CORA were merged with TOPEX/POSEIDON (T/P), Jason, ERS-1/2, and Envisat SLA data distributed by the Collecte Localisation Satellites (CLS) Space Oceanography Division. Its surface-driven wind data were obtained from the NCEP reanalysis products and QuikSCAT.

The AIPO1.0 system adopted the Hybrid Coordinate Ocean Model (HYCOM) and the Ensemble Optimal Interpolation (EnOI) scheme as its ocean model and assimilation scheme, respectively (Yan et al., 2010a). Assimilated data included the *in situ* hydrographic data from ENSEMBLES (EN3 version 1d) (Ingleby and Huddleston, 2007) and SLA mapped on a $(1/3)^\circ \times (1/3)^\circ$ Mercator grid from CLS and satellite SST products (Reynolds et al., 2007). The EN3 dataset contained WOD05, GTSPP, Argo profiles, and Arctic Synopic Basin-wide Oceanography (ASBO). The daily product of AIPO1.0 had the highest time resolution among the seven datasets.

The *in situ* hydrographic data along the 18°N, 12.75°N, and 120°E sections in the SCS were collected during the open cruises in the northern South China Sea in the period 2005–08, which were implemented by the South China Sea Institute of Oceanology, Chinese Academy of Sciences, and the South China Sea Monsoon Experiment in 1998 (SCSMEX98). During these cruises, temperature–salinity data at the site were measured with a CTD recorder and the vertical interval of the data was 1 m. The *in situ* data of every section were collected over a period of several days. For example, during the open cruise in the northern South China Sea in 2005, measurement of data in the 18°N section was continued from 10 September to 16 September. We used this measurement as a proxy of the corresponding month and compared it with other monthly datasets.

The analysis area in this study was the SCS basin (0°–25°N, 99°–121°E) without the Sulu Sea. Vertically integrated temperature of the upper 300 m was studied as a proxy of the upper OHC. A depth of 300 m was chosen because it was close to the middle of the main thermocline (Carol and Thompson, 2000). As the estimates of the OHC were not sensitive to the vertical resolutions of the upper ocean (figures are not shown here), the results from different datasets with various vertical resolutions were comparable. The OHC was calculated with the original levels of each dataset. In order to maintain a consis-

tency in the time span of measurement, we chose a common period of 14 years (1993–2006) for all these datasets. Monthly climatological upper OHC data of each grid were obtained by averaging individual calendar months during the 14 years. Space-averaged upper OHC of the SCS was calculated as the mean value of all grids, and interannual space-averaged upper OHC anomalies in the SCS were obtained by subtracting the monthly climatology of space-averaged upper OHC.

3. Results of Comparisons

3.1 *Climatology state of the upper OHC anomalies in the SCS*

First, the annual cycles of the upper OHC anomalies averaged over the SCS from the seven datasets were compared. As shown in Fig. 2, the upper OHC anomalies were found to be positive during May–November and negative during December–April. All these datasets showed that the upper OHC was minimum in February, whereas the month in which it became maximum varied from dataset to dataset. WOA09, SODA, GODAS, and CORA indicated that the upper OHC reached a maximum value in October. WOA09 and CORA also exhibited another peak in July, in addition to the peak in October; however, this phenomenon was not observed in other datasets. For Ishii and OFES, the values of the upper OHC in June–October were almost the same, and the peaks were obscure. In terms of the annual cycle, most of these datasets performed consistently, although the months in which the upper OHC reached the maximum value varied slightly.

In this study, April, July, October, and January represented boreal spring, summer, autumn, and winter, respectively. Figures 3–6 display the seasonal distribution of the upper OHC anomalies over the SCS. In spring (Fig. 3), the spatial distribution of the upper OHC anomalies were not uniform. Positive anomalies appeared in the central SCS basin, with a warm core off the east coast of Vietnam. In the northern part and south of 10°N, the anomalies were found to be negative generally. In summer, the positive center moved northward to about 18°N off the southwest of the Luzon Strait, and another mild warm center was created off the southeast Vietnam coast (Fig. 4). OFES, SODA, GODAS, CORA, and AIPO1.0 showed negative anomalies along the Hainan Island and the east Vietnam coast. Ishii and WOA09 had no data near the Hainan Island and the east Vietnam coast, so this phenomenon was not observed in case of Ishii and WOA09. The situation in autumn was a little complex compared with other seasons. All the seven datasets presented a cold core off the Vietnam coast and a warm core off the west of the Luzon Strait. The autumn patterns calculated from OFES and GODAS were similar (Fig. 5). A negative region located between about 11°N and 18°N was embedded between two positive regions. In addition, Ishii, CORA, and WOA09 showed a slender warm area in the southeast basin of the SCS. In winter, almost the entire basin of the SCS showed negative anomalies, except for some coastal areas. There were two obvious cold anomaly centers: the larger and stronger one existed at the west of the Luzon Strait, and the smaller and weaker one was located southeast of the Indo-China Peninsula (Fig.6).

Considering variations over the entire SCS, the annual cycle of the upper OHC were mainly subjected to surface heat flux and heat advection through straits. Surface heat flux was the dominant heat process dur-

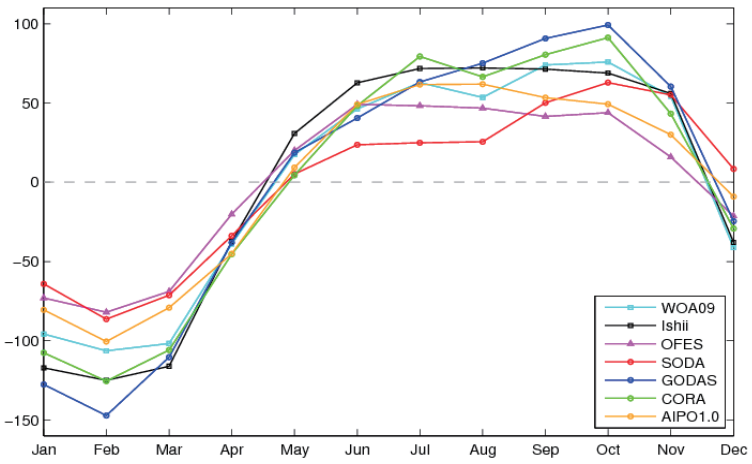

Fig. 2. Annual cycle of OHC anomalies calculated from seven analyses, which were averaged spatially over the whole SCS (units: °C m).

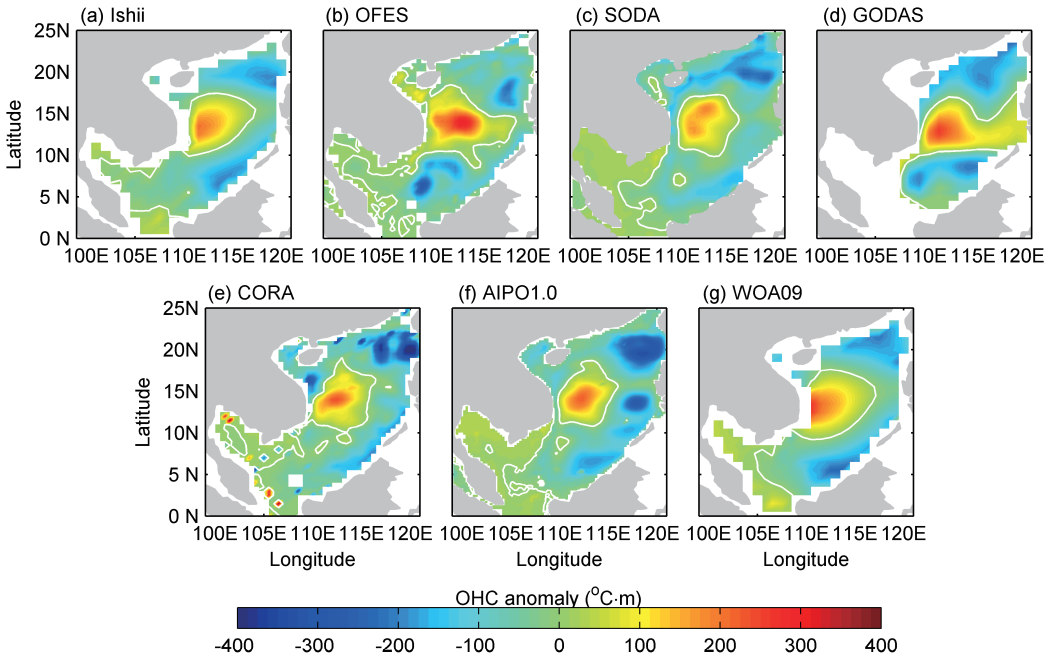

Fig. 3. Distribution of the climatological anomalies of OHC over the SCS in spring.

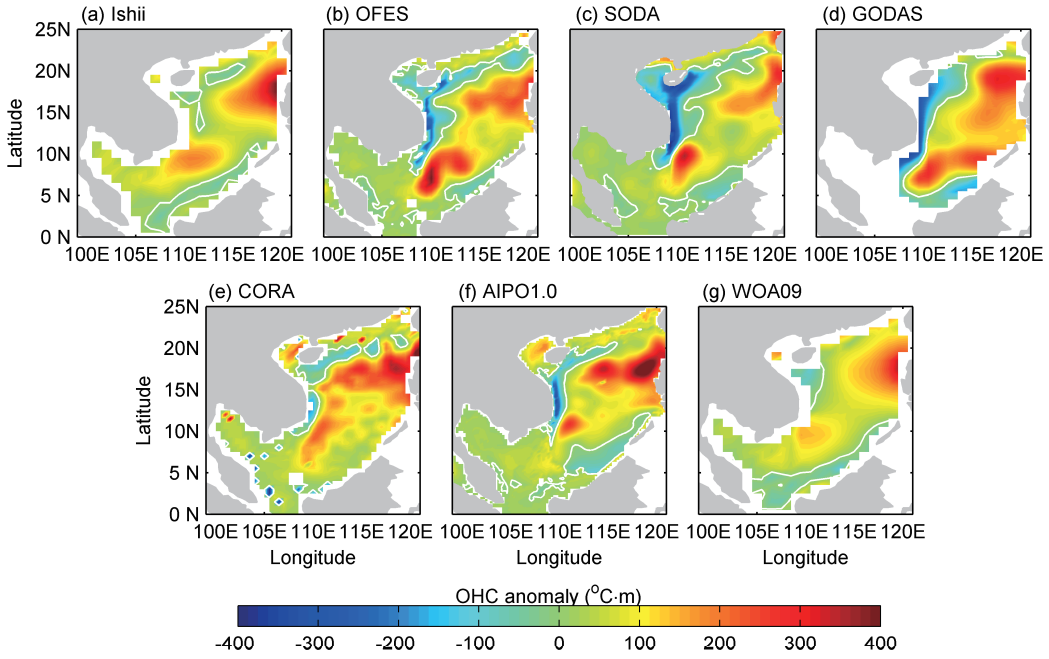

Fig. 4. The same as Fig. 3, but for summer.

ing late spring to early fall. In winter, however, heat advection appeared to be the primary process responsible for the cooling of the upper layer of the SCS (Qu et al., 2004). For local variations, other processes such as surface wind curl and baroclinic Rossby waves were also important (Liu et al., 2001). Overall, the climatology state of the upper OHC anomalies in the SCS revealed by the seven datasets resembled each other.

3.2 *Interannual variability and Taylor diagram*

In addition to the annual cycle, the interannual variability of the upper OHC in the SCS was also distinct (Fig. 7). Overall, the curves of Ishii and CORA were quite similar; both had two peaks in 1999 and 2006, which were consistent with the thermosteric sea

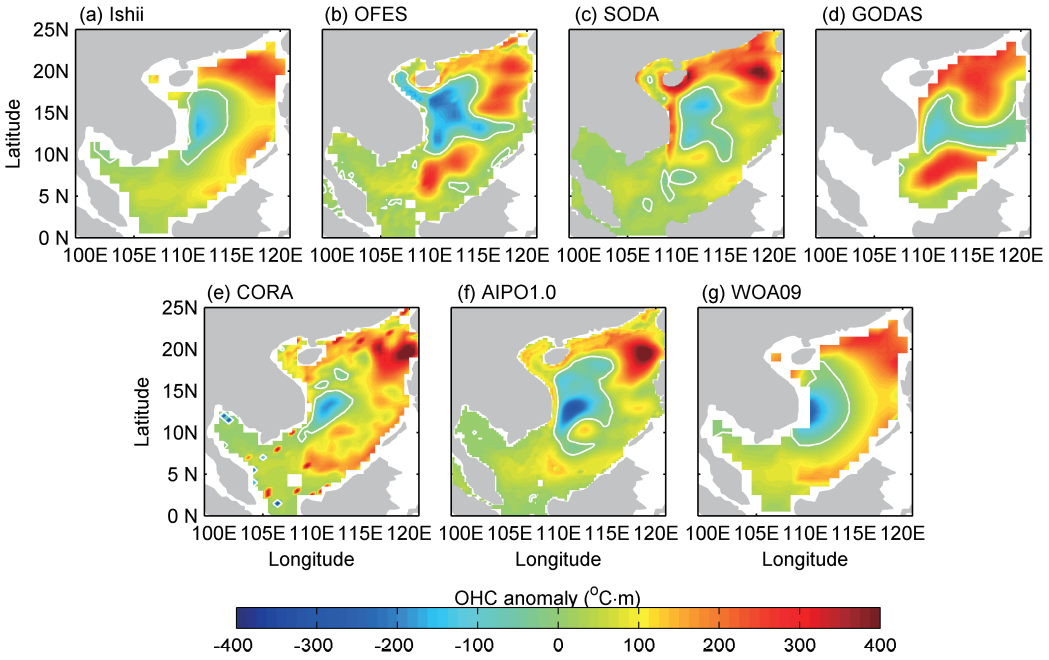

Fig. 5. The same as Fig. 3, but for autumn.

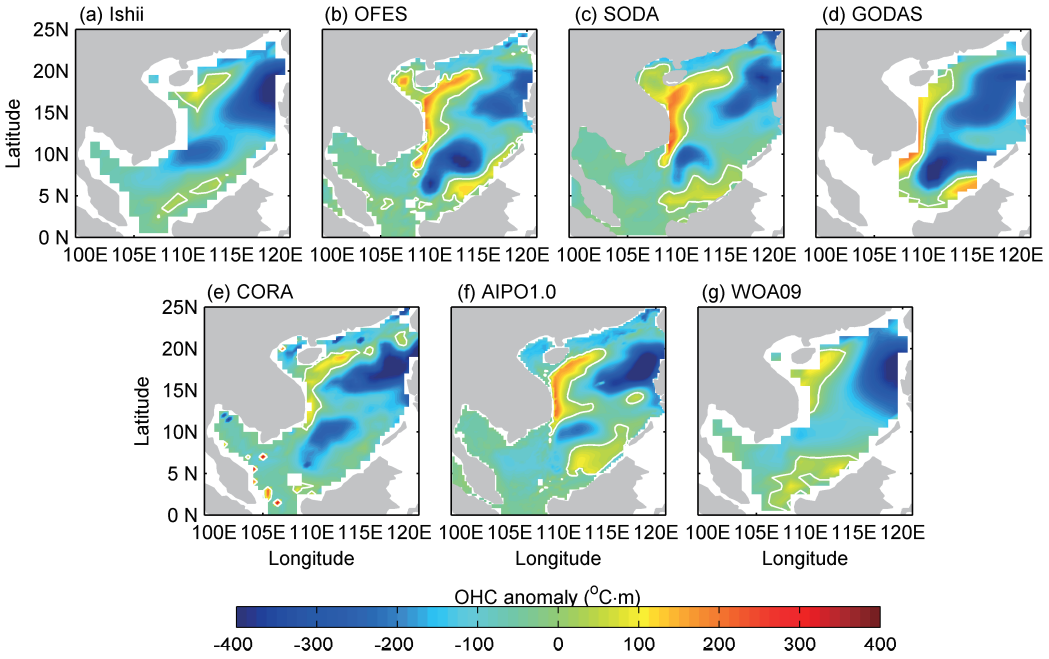

Fig. 6. The same as Fig. 3, but for winter.

level variations (Cheng and Qi, 2007; Rong et al., 2007). For GODAS, the large amplitude of the upper OHC could partly be attributed to the lack of data in the shallow water (shallower than 100 m). We calculated the upper OHC over the areas deeper than 100 m from other datasets and found larger amplitudes in all cases became (figures are not shown), indicating that the upper OHC over the deep water had stronger interannual variability than that in shallow water. However, the amplitude of GODAS was still the largest, suggesting that there might be other reasons for its large value. Some previous researches reported the upper OHC in the SCS to be negative (positive) during El Niño (La Niña) events (Cheng and Qi, 2007; Rong et al., 2007; Yan et al., 2010b), so it was supposed to have a peak in 1999. However, SODA and OFES had

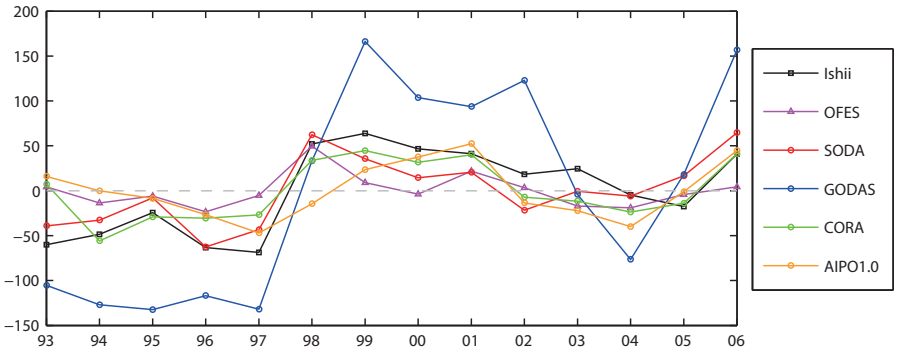

Fig. 7. Interannual variations of the space-averaged OHC anomalies in the SCS. The bottom axis is time (year) and the y axis is the OHC anomalies in units of °C m.

an abnormal peak in 1998 instead of 1999, and the reason is unclear. In AIPO1.0, the upper OHC reached a maximum value not in 1999 but in 2001, which agreed with the variation of SLA over the SCS (Cheng and Qi, 2007).

In order to compare quantitatively the performances of these datasets in presenting the interannual variability of the upper OHC in the SCS, we adopted a Taylor diagram. A Taylor diagram is able to plot and compare various aspects of numerous datasets on a single diagram. Because Ishii is an objective analysis dataset, without any ocean model or data assimilation, and has already been used successfully to study the OHC in the SCS (Cheng and Qi, 2007; Rong et al., 2007; Yan et al., 2010a, b), we chose Ishii as a reference for comparison. In the Taylor diagram, three kinds of statistical variables were considered: standard deviations of each dataset, centered pattern root mean square differences (RMSD), and correlation coefficients. As shown in Fig. 8, the distance from a point in a dataset to the origin was represented as the standard deviation (if the point in a dataset was nearer to the origin than that in Ishii, this dataset was considered to have a higher variance). The correlation coefficients between Ishii and other datasets were shown along the outer arc of the diagram as a function of the angle from the vertical axis. From this diagram, it could be found out whether the patterns of the other datasets were similar to that of Ishii. The distances between the Ishii point and the points in other datasets represented the RMSD (Taylor, 2001), which took both the patterns and the variances amplitude into account.

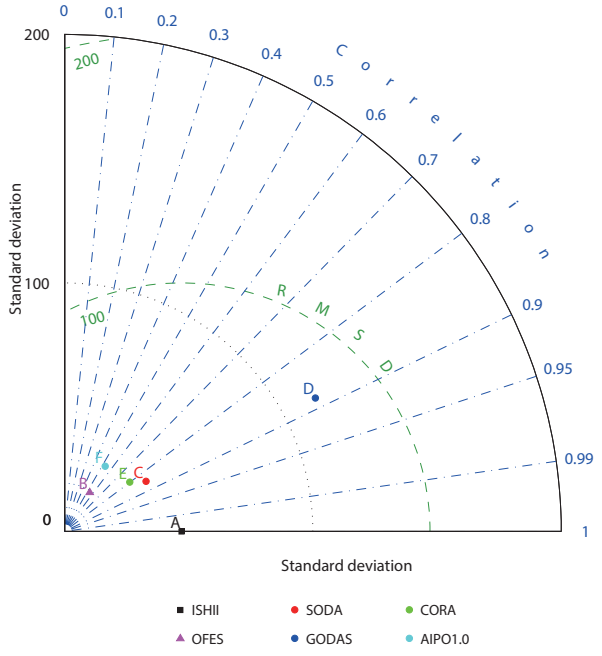

Fig. 8. Taylor diagram for annual average OHC anomalies from six analyses.

In the Taylor diagram (Fig. 8), the standard deviations of SODA, CORA, and AIPO1.0 were similar, although they were slightly weaker than that of Ishii. OFES and GODAS had the smallest and largest variances amplitudes, respectively. CORA, SODA, and GODAS had the highest correlation coefficient (with a value of more than 0.8) with Ishii, indicating their similar patterns. Considering both variance amplitude and correlation, RMSD indicated that SODA had the best correspondence with Ishii.

3.3 *Comparisons with cruise observations*

In order to evaluate different datasets, they were required to be compared with observations. The capabilities of these datasets in presenting the upper OHC depended to a large extent on how well they can simulate the vertical structure of temperature. Direct comparisons with in situ temperature measurements were conducted, including the temperature pro-

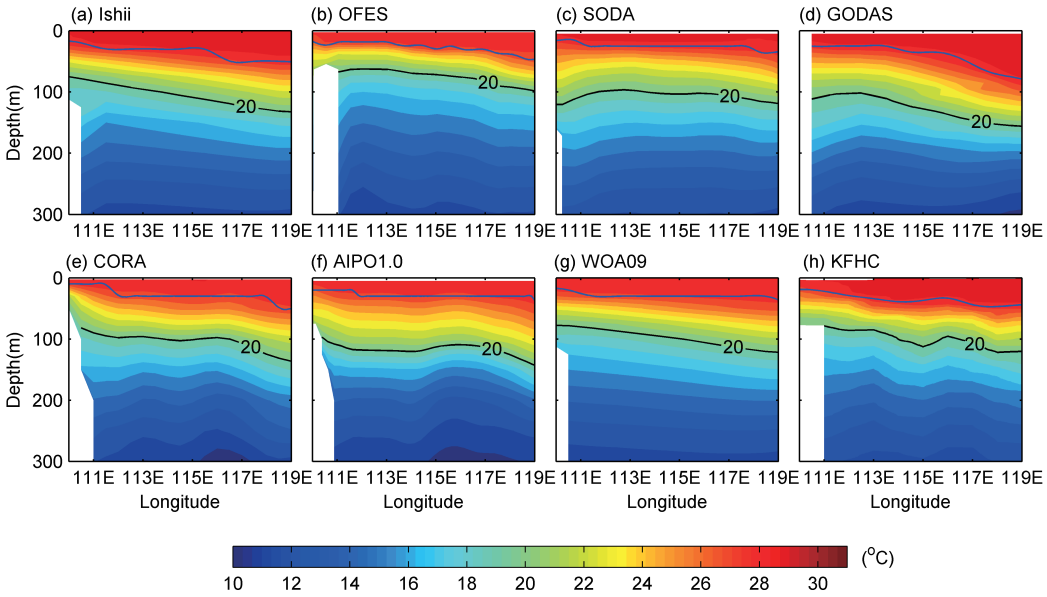

Fig. 9. Mean state of vertical temperature section along the 18°N section in the SCS from seven datasets and observations during 2005–08, except AIPO1.0 for which the time span was 2005–06. The blue lines indicate the lower bounds of the mixed layer and the black lines indicate the Z20.

files along the 18°N (110°–119°E), 12.75°N (110.5°–119.5°E), and 120°E (16.5°–22.5°N) sections. In the vertical structure of temperature, both the depths of the thermocline and the mixed layer were important references of the dynamic processes in the upper ocean. For comparison, the 20°C isotherms (Z20) and lower bounds of mixed layers were plotted. The Z20 depth was chosen as a reference because of its typicality in presenting mid-thermocline isotherm in the tropical ocean (Schott et al., 2009). The lower bound of mixed layer was defined as the depth whose temperature was lower than that of near-surface layer (10 m) by 0.8°C (Liu et al., 2007).

The open cruise of northern South China Sea started in 2004 and has been conducted every year since then. So far, more than five years of hydrologic data along the 18°N section in August and September were collected, from which a climatology mean state could be obtained. As the depths of most of the stations were shallower than 150 m in 2004, the hydrologic data of that year were not used to get the climatologic state. In order to maintain a high consistency in the time span of study across all datasets, we chose a four-year period (2005–08) and then estimated their mean states in August and September. Besides, the OFES data of 2007 and 2008 used here are from its version of 0.1°×0.1°. In the climatologic state of temperature along the 18°N section (Fig. 9), the mixed layers and Z20s of the seven datasets were roughly consistent with the observations, which sloped downward toward the east. Among these datasets, Ishii and CORA performed very well. For OFES, the mixed layer was thinner and the depth of Z20 was shallower. The performance of SODA was unsatisfactory, as its mixed layer was thinner and the slope of Z20 did not match well with the observational data. The mixed layer of GODAS in the east was thicker than in situ measurement. The slopes of the mixed layers for AIPO1.0 and WOA09 were not same as the observations.

During May of 1998, the isotherms along the 12.75°N (110.5°–119.5°E) section sloped slightly downward toward the east from 111°E to 116°E and upward from 116°E to 119°E in upper 100 m (Fig. 10). The mixed layers of CORA and AIPO1.0 were thinner than observations. The mixed layer of OFES was cooler than the observed values. The Z20s of OFES, CORA, and AIPO1.0, especially those of CORA and AIPO1.0, were more consistent with the observations, indicating their better performances in presenting the upper ocean response to winds (Fig. 10).

To validate the performances of these datasets in presenting the vertical structure of temperatures in complicated sea areas, the 120°E (16.5°–22.5°N) section (Fig. 11) was chosen for comparison. This section was located near to the Luzon Strait, where water exchanges were (Qu et al., 2004). In spite of the complexity of this area, OFES captured the main characteristics of the vertical structure of temperatures well. The Z20 sloped downward toward the north at about 21°N, whereas the isotherms above it showed a dome

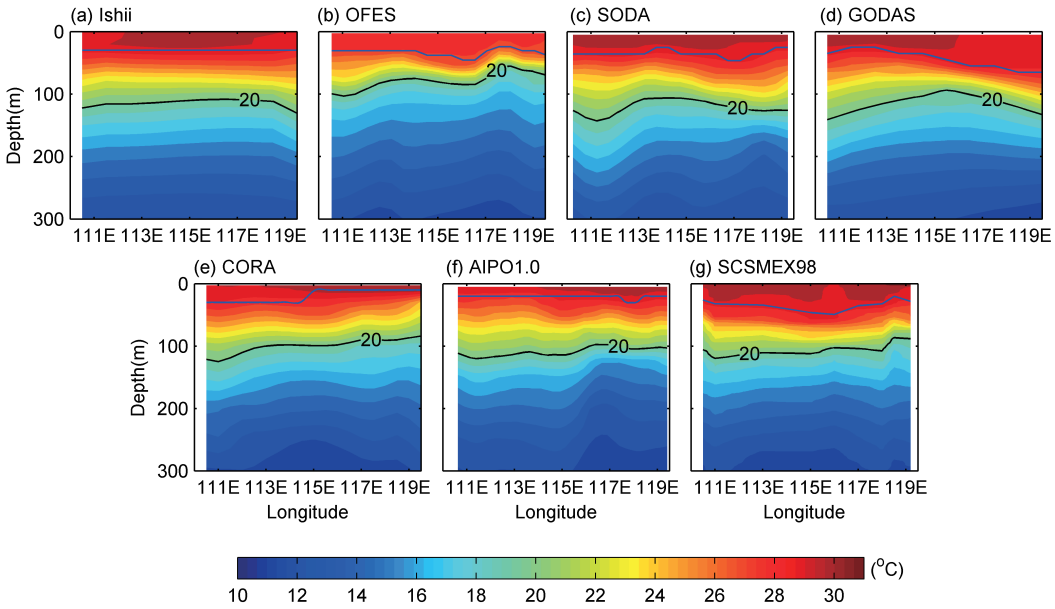

Fig. 10. Vertical sections of temperature along the 12.75°N section in the SCS from six analyses and observations in May of 1998. The blue lines represent the lower bounds of the mixed layer and the black lines represent the Z20.

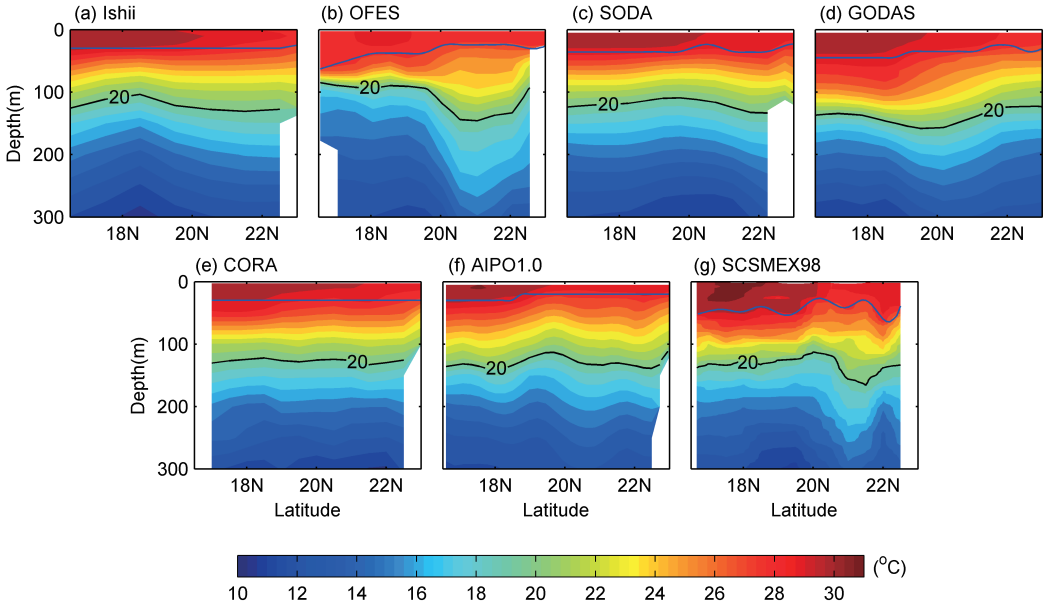

Fig. 11. The same as Fig. 6, but for June of 1998 along the 120°E section in the SCS.

almost at the same latitude. AIPO1.0 could roughly present these characteristics, although its mixed layer was thinner than observations. The performances of other datasets were unsatisfactory.

As shown in Figs. 9–11, none of the Z20s were deeper than 200 m, proving that the depth of 300 m was suitable for presenting the upper OHC variability in the SCS. The Z20s of Ishii, OFES, CORA, and AIPO1.0 were similar to those of in situ hydrologic data, while GODAS and SODA showed larger deviations from the observations.

4. Summary

This study provides a systematic validation of the performances of multiocean datasets, including

Ishii, OFES, SODA, GODAS, CORA, AIPO1.0, and WOA09, in presenting the upper OHC in the SCS during 1994–2006.

As a whole, the seven datasets performed consistently in presenting the annual cycle of the upper OHC, which attained a maximum value in October. The central deep basin, southwest of the Luzon Strait, and the west boundary areas were found to have large annual amplitudes.

For the interannual variations, the performances of these datasets were different, especially their responses to ENSO events. Take 1997/98 El Niño for example, SODA and OFES showed peaks in 1998, while Ishii, OFES, and CORA did so in 1999. According to the Taylor diagram, SODA, GODAS, and CORA were more consistent with Ishii et al. (2006).

Compared with in situ observations along selected sections, the depths of mixed layers in most datasets were shallower. The Z20s of Ishii, OFES, CORA, and AIPO1.0 were more consistent with the observations, indicating their good responses to wind.

The objective analysis dataset, Ishii, was used to calculate the upper OHC in the SCS. Because of its long time span, it can be used to study the long-term variations in upper OHC in the SCS. However, Ishii could not present the vertical structure well. Considering the responses to ENSO, CORA has the best consistence with Ishii. The high resolutions of OFES and AIPO1.0 were essential for the study of mesoscale ocean progresses. Besides, OFES was found to be good at describing the vertical structure of temperatures in the SCS. The performance of SODA in Taylor diagram was better than that in presenting the vertical structure of temperature. Understanding the performances of these datasets would be helpful for oceanographers to choose the suitable one for investigating the OHC in the SCS.

Acknowledgements. This study was supported by the National Basic Research Program of China (Grant Nos. 2010CB950400 and 2013CB430301), the National Natural Science Foundation of China (Grant Nos. 41276025 and 41176023), and the R&D Special Fund for Public Welfare Industry (Meteorology) (Grant No. GYHY201106036). The OFES simulation was conducted on the Earth Simulator under the support of JAMSTEC. The hydrologic data were obtained during the open cruises in the northern South China Sea in the period 2005–08, which were supported by the Data Sharing Infrastructure of Earth System Science–Data Sharing Service Center of the South China Sea and adjacent regions. Constructive remarks by two anonymous reviewers are greatly appreciated.

REFERENCES

Behringer, D. W., 2005: The global ocean data assimilation system (GODAS) at NCEP. Preprints, 11th Symp. on Integrated Observing and Assimilation Systems for the Atmosphere, Oceans, and Land Surface (IOAS-AOLS), San Antonio, TX, American Meteorological Society, 3.3.[Available online at http://ams.confex.com/ams/pdfpapers/119541.pdf.]

Carol, L., and L. Thompson, 2000: Formation mechanisms for North Pacific central and eastern subtropical mode waters. *J. Phys. Oceanogr.*, **30**, 868–887, doi: 10.1175/1520-0485(2000)030<0868:FMFNPC>2.0.CO;2.

Carton, J. A., and A. Santorelli, 2008: Global decadal upper-ocean heat content as viewed in nine analyses. *J. Climate*, **21**, 6015–6035, doi: 10.1175/2008JCLI2489.1.

Carton, J. A., and B. S. Giese, 2008: A reanalysis of ocean climate using simple ocean data assimilation (SODA). *Mon. Wea. Rev.*, **136**(8), 2999–3017, doi: 10.1175/2007mwr1978.1.

Cheng, X., and Y. Qi, 2007: Trends of sea level variations in the South China Sea from merged altimetry data. *Global and Planetary Change*, **57**(3–4), 371–382, doi: 10.1016/j.gloplacha.2007.01.005.

Domingues, C. M., J. A. Church, N. J. White, P. J. Gleckler, S. E. Wijffels, P. M. Barker, and J. R. Dunn, 2008: Improved estimates of upper-ocean warming and multi-decadal sea-level rise. *Nature*, **453**(7198), 1090–1093, doi: 10.1038/nature07080.

Douglass, D. H., and R. S. Knox, 2009: Ocean heat content and Earth's radiation imbalance. *Physics Letters* (*A*), **373**(36), 3296–3300, doi: 10.1016/j.physleta.2009.07.023.

He, Y., and C. Guan, 1997: Interannual and interdecadal variability in heat content of the upper ocean of the South China Sea. *Journal of Tropical Oceanography*, **16**(1), 23–29. (in Chinese)

Ingleby, B., and M. Huddleston, 2007: Quality control of ocean temperature and salinity profiles—Historical and real-time data. *J. Mar. Syst.*, **65**(1–4), 158–175, doi: 10.1016/j.jmarsys.2005.11.019.

Ishii, M., M. Kimoto, K. Sakamoto, and S.-I. Iwasaki, 2006: Steric sea level changes estimated from historical ocean subsurface temperature and salinity analyses. *Journal of Oceanography*, **62**(2), 155–170, doi: 10.1007/s10872-006-0041-y.

Kalnay, E., and Coauthors, 1996: The NCEP/NCAR 40-year reanalysis project. *Bull. Amer. Meteor. Soc.*, **77**(3), 437–471.

Kubotam, M., N. Iwasaka, S. Kizu, M. Konda, and K. Kutsuwaka, 2002: Japanese ocean flux data sets with use of remote sensing observations (J-OFURO). *Journal of Oceanography*, **58**, 213–225.

Lai, Z., S, Peng, Y. Li, and Q. Liu, 2011: Relationship between summer monsoon outbreak and upper-ocean heat content anomalies over the South China Sea. *Journal of Tropical Oceanography*, **30**(6), 47–56. (in

Chinese)

Levitus, S., J. I. Antonov, J. Wang, T. L. Delworth, K. W. Dixon, and A. J. Broccoli, 2001: Anthropogenic warming of Earth's climate system. *Science*, **292**(5515), 267–270, doi: 10.1126/science.1058154.

Levitus, S., J. I. Antonov, T. P. Boyer, R. A. Locarnini, H. E. Garcia, and A. V. Mishonov, 2009: Global ocean heat content 1955–2008 in light of recently revealed instrumentation problems, *Geophys. Res. Lett.*, **36**(7), L07608, doi: 10.1029/2008gl037155.

Liu, Z., H. Yang, and Q. Liu, 2001: Regional dynamics of seasonal variability in the South China Sea. *J. Phys. Oceanogr.*, **31**, 272–284.

Liu, H., L. Jiang, Y. Qi, Q.Mao, and X. Cheng, 2007: Seasonal variabilities in mixed layer depth in the Nansha Islands Sea area. *Advances in Marine Science*, **25**(3), 268–279. (in Chinese)

Lyman, J. M., S. A. Good, V. V. Gouretski, M. Ishii, G. C. Johnson, M. D. Palmer, D. M. Smith, and J. K. Willis, 2010: Robust warming of the global upper ocean. *Nature*, **465**(7296), 334–337, doi: 10.1038/nature09043.

Masumoto, Y., and Coauthors, 2004: A fifty-year eddy-resolving simulation of the world ocean: Preliminary outcomes of OFES (OGCM for the Earth simulator), *Journal of the Earth Simulator*, **1**, 35–56.

Na, H., K.-Y. Kim, K.-I. Chang, J. J. Park, K. Kim, and S. Minobe, 2012: Decadal variability of the upper ocean heat content in the East/Japan Sea and its possible relationship to northwestern Pacific variability. *J. Geophys. Res.*, **117**, C02017, doi: 10.1029/2011jc007369.

Qu, T., Y. Y. Kim, M. Yaremchuk, T. Tozuka, A. Ishida, and T. Yamagata, 2004: Can Luzon Strait transport play a role in conveying the impact of ENSO to the South China Sea? *J. Climate*, **17**, 3644–3657.

Reynolds, R. W., T. M. Smith, C. Liu, D. B. Chelton, K. S. Casey, and a. M. G. Schlax, 2007: Daily high-resolution analyses for sea surface temperature. *J. Climate*, **20**, 5473–5496, doi: 10.1175/2007JCLI1824.1.

Rong, Z., Y. Liu, H. Zong, and Y. Cheng, 2007: Interannual sea level variability in the South China Sea and its response to ENSO. *Global and Planetary Change*, **55**(4), 257–272, doi: 10.1016/j.gloplacha.2006.08.001.

Rosati, A., and K. Miyakoda, 1988: A general circulation model for upper ocean simulation. *J. Phys. Oceanogr.*, **18**, 1601–1626.

Sasai, Y., A. Ishida, Y. Yamanaka, and H. Sasaki, 2004: Chlorofluorocarbons in a global ocean eddy-resolving OCCM: Pathway and formation of Antarctic Bottom Water. *Geophys. Res. Lett.*, **31**(12), L12305, doi: 10.1029/2004GL019895.

Sasaki, H., Y. Sasai, S. Kawahara, M. Furuichi, F. Araki, A. Ishida, Y. Yamanaka, Y. Masumoto, and H. Sakuma, 2004: A series of eddy-resolving ocean simulations in the world ocean—OFES (OGCM for the Earth Simulator) project. OCEAN'04. MTTS/IEEE TECHNO-OCEAN'04, 1535–1541.

Sasaki, H., M. Nonaka, Y. Masumoto, Y. Sasai, H. Uehara, and H. Sakuma, 2006: An eddy-resolving hindcast simulation of the quasi-global ocean from 1950 to 2003 on the Earth Simulator. *High Resolution Numerical Modelling of the Atmosphere and Ocean*, W. Ohfuchi and K. Hamilton, Eds., Springer, New York, 157-185.

Schott, F. A., S.-P. Xie, and J. P. McCreary, 2009: Indian Ocean circulation and climate variability. *Rev. Geophys.*, **47**(1), doi: 10.1029/2007rg000245.

Taylor, K. E., 2001: Summarizing multiple aspects of model performances in a single diagram. *J. Geophys. Res.*, **106**, 7183–7192.

Tong, J., J. Wang, and Y. Qi, 2006: Interannual variability of the heat storage anomaly in the South China Sea estimated from merged altimetric data. *Chinese Journal of Geophysics*, **49**(6), 1651–1656. (in Chinese)

Wang, B., and R. Wu, 1997: Peculiar Temporal Structure of the South China Sea summer monsoon. *Adv. Atmos. Sci,*, **14**(2), 177–194.

Wang, G., J. Su, Y. Ding, and D. Chen, 2007: Tropical cyclone genesis over the south China sea. *J. Mar. Syst.*, **68**(3–4), 318–326, doi: 10.1016/j.jmarsys.2006.12.002.

Yan, C., J. Zhu, and J. Xie, 2010a: An ocean reanalysis system for the joining area of Asia and Indian-Pacific ocean. *Atmos. Oceanic Sci. Lett.*, **3**(2), 81–86.

Yan, Y., Y. Qi, and W. Zhou, 2010b: Interannual heat content variability in the South China Sea and its response to ENSO. *Dynamics of Atmospheres and Oceans*, **50**(3), 400–414, doi: 10.1016/j.dynatmoce.2010.07.002.

Zhu, J., B. Huang, and M. A. Balmaseda, 2011: An ensemble estimation of the variability of upper-ocean heat content over the tropical Atlantic Ocean with multi-ocean reanalysis products. *Climate Dyn.*, **39**(9), doi: 10.1007/s00382-011-1189-8.